Journal of Molecular Catalysis A: Chemical 324 (2010) 64–74

Contents lists available at ScienceDirect

Journal of Molecular Catalysis A: Chemical

journal homepage: www.elsevier.com/locate/molcata

Computational catalysis

On the nature of the active site in ruthenium olefin coordination–insertion polymerization catalysts☆

Wouter Heyndrickx, Giovanni Occhipinti, Yury Minenkov, Vidar R. Jensen*

Department of Chemistry, University of Bergen, Allégaten 41, N-5007 Bergen, Norway

ARTICLE INFO

Article history:
Received 22 January 2010
Accepted 18 March 2010

Keywords:
Density functional theory
Homogeneous catalysis
Olefin polymerization
Ruthenium

ABSTRACT

The only ruthenium-based catalyst for olefin polymerization reported in the open scientific literature is a (bis(oxazoline)pyridine)$RuCl_2$(ethylene) complex (**I**) which, upon treatment with methyl aluminoxane (MAO), displays low activity for ethylene homopolymerization and copolymerization [35]. Analogy to other MAO-activated catalysts suggests that the active species should be a [(bis(oxazoline)pyridine)RuMe(ethylene)]$^+$ (**II**) cation. However, the structurally similar [(bis(imino)pyridine)RuMe(ethylene)]$^+$ (**III**) complex was found to be inactive [28]. A density functional theory (DFT) investigation of direct ethylene insertion into the metal–propyl bond in cationic ruthenium complexes bearing the bis(oxazoline)pyridine ("pybox") and bis(imino)pyridine ligands shows that the activity of **I**/MAO and inactivity of **III** cannot be explained by differences in the insertion barriers for such cations. This indicates that the catalytic activity of **I**/MAO must originate from an active species different from **II**. An extensive search for the active species of **I**/MAO, involving a range of different polymerization mechanisms and metal oxidation states did not result in calculated barriers to chain growth significantly lower than that for **III**, suggesting that the latter is not due to a mononuclear ruthenium complex carrying an intact pybox ligand.

1. Introduction

More than 50 years after the discovery of the Ziegler–Natta catalysts [1,2], the quest for new insertion–coordination catalysts is still ongoing and is propelled by the goal to develop active, selective and inexpensive catalysts that provide extended control over the polymer structure.

The most prominent olefin polymerization catalysts are based on early, electron deficient transition metals such as Ti^{IV} and Zr^{IV}. The electron deficiency of the metal is generally believed to contribute to high activity [3,4]. However, during the last decade, partly due to the sensitivity of these electron deficient catalysts to oxygen and polar functional groups, olefin polymerization using late transition metals has attracted a lot of interest [5], resulting in catalysts based on a variety of transition metals [6,7]. Late-metal polymerization catalysts are not only more robust towards impurities, they also allow for the copolymerization of ethylene with polar monomers. This is an attractive goal, since the incorporation of polar groups in the polymer structure opens the possibility for obtaining and tuning a range of polymer properties such as crystallinity, toughness, adhesion, and other surface properties [8,9].

Despite several important breakthroughs realized during the last 15 years in the field of late transition metal catalyzed polymerization [10–27], the challenge which currently stimulates intense research activity worldwide is to achieve high activity, functional group tolerance and the ability to copolymerize ethylene with polar monomers in one and the same catalytic system.

A notable example of late transition metal polymerization catalysts are the very active and inexpensive bis(imino)pyridine Fe and Co catalysts that were discovered simultaneously by the Brookhart and Gibson groups [23,24,27], but these do not copolymerize ethylene with methyl acrylate [25,26]. Following the discovery of the Fe and Co bis(imino)pyridine catalysts, Dias et al. investigated the second-row analogues based on Ru and Rh [28]. An extension of the work on iron and cobalt to ruthenium in particular seemed appropriate. The excellent functional group tolerance and low moisture- and air-sensitivity of the ruthenium olefin metathesis catalysts [29] makes this metal stand out as an appealing candidate catalyst also for olefin polymerization. Furthermore, this metal possesses flexible coordination chemistry and is also not among the most expensive of the transition metals. Ruthenium has thus been the subject of considerable interest as a potential olefin polymerization catalyst in recent years, reflected, among other things, in a number of patents [30–34]. Unfortunately, the methyl ethylene

☆ This paper is part of a special issue on Computational Catalysis.

* Corresponding author. Tel.: +47 555 83489; fax: +47 555 89490.
E-mail address: Vidar.Jensen@kj.uib.no (V.R. Jensen).

1381-1169/$ – see front matter © 2010 Elsevier B.V. All rights reserved.
doi:10.1016/j.molcata.2010.03.023

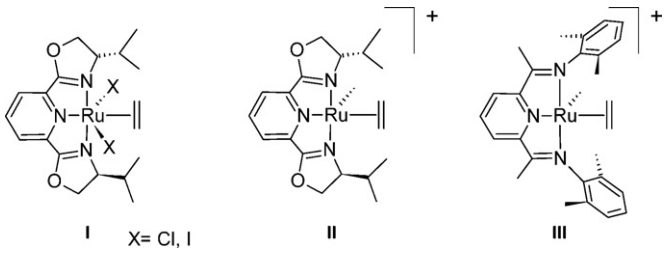

I II III

Chart 1. The Nomura catalyst **(I)** [35–37], the methyl ethylene cation **(II)** supposedly generated by MAO upon activation of **I**, and the corresponding Brookhart complex **(III)** [28].

bis(imino)pyridine Ru complex developed in the Brookhart group (structure **III**, Chart 1, in the following termed the "Brookhart complex") with tetrakis[3,5-bis(trifluoromethyl)phenyl]borate as counterion showed no activity towards ethylene insertion [28]. In contrast, upon activation with methyl aluminoxane (MAO), the structurally very similar bis(oxazoline)pyridine ("pybox") catalysts of Nomura et al. [35–37], in the following termed the "Nomura catalyst", do show activity, albeit low, towards ethylene homopolymerization and copolymerization with non-polar olefins. The generally expected role of MAO is to promote both methylation of the metal and dissociation of one or more halide ligands [38]. Puzzlingly, for the pybox catalyst precursors, these initiation processes should lead to a structural analogue (structure **II**, Chart 1) of the inactive Brookhart complex **III**.

A more probable explanation for the contrasting catalytic properties of the Brookhart complex and the Nomura catalyst is the fact that the role of MAO may be more involved than the standard activation described above. MAO has been claimed to be responsible for reducing, ionizing, and methylating polymerization catalyst precursors, or a combination of these processes. A particularly complicated example is offered by the related Fe bis(imino)pyridine catalysts, which also require MAO activation, and where the exact nature of the active species has been subject to much debate. The active catalyst has been suggested to consist of everything from dicationic [39,40], monocationic [41–45], neutral [46,47], to anionic [48] complexes, with the corresponding formal oxidation states ranging from Fe^{III}, Fe^{II}, Fe^{I}, to Fe^{0}, respectively. And again, the observed catalytic activity has also been ascribed to the presence of combinations of such individual, well-defined centers [49–53]. The wide range of possible formal iron oxidation states is partly related to the ability of the bis(imino)pyridine ligand to serve as a single- or two-electron acceptor [54–56]. The situation is further complicated by the formation of bimetallic Fe–Al complexes following MAO activation [57–60]. Additional possibilities involve alkylation of the bis(imino)pyridine ligand at various positions [61–67], protonation or deprotonation of the ligand [56,63,68,69], dimerization of the ligand [63,70] or bidentate coordination of the ligand [71,72]. Hence, the possibility that the catalytically active species following MAO activation in the Nomura catalyst is, in fact, not the anticipated structure **II** (Chart 1), cannot be excluded. The case for a modified (i.e., different from **II**) active species is supported by the low activity recorded for the Nomura catalyst (0.5–2 g/mmol Ru h) and the high molecular weight of the resulting polyethylene ($M_w = 2 \times 10^6$) [35], which, taken together, indicate that only a small fraction of the Ru centers are active.

The possibility that mono- or dinuclear Al complexes are responsible for the observed activity of the Nomura catalyst is considered to be unlikely, as a blank polymerization run yielded no polymer [35]. A ligand transfer from Ru to Al could be imagined [73], but the resulting Al bis(imino)pyridine complex was shown to be inactive [74]. Other Al polymerization catalysts are known [67,75], but mono- and dinuclear Al species were found to be unlikely to yield high molecular weight polymer [76–78].

In order to identify the most likely active centers and catalytic mechanisms of the Nomura catalyst, we have investigated several different reaction pathways for ethylene polymerization in combination with a range of Ru species (dicationic, monocationic, neutral, and anionic). The thus calculated barriers to chain growth have been routinely compared to corresponding insertion barriers calculated for the well-defined but inactive Brookhart complex. We have thus been able to discard as unlikely those reaction routes for which the calculated barriers are comparable to or higher than the ones obtained for the Brookhart complex. It should be noted that identification of the active species of the Nomura catalyst not only is of interest from a fundamental point of view, but also would open the possibility for insight-driven development of more active Ru-based polymerization catalysts. The excellent functional group tolerance shown by ruthenium in olefin metathesis (*vide supra*) suggests that it should, simultaneously, be possible to achieve ruthenium-based catalysts for copolymerization of ethylene with polar vinyl monomers, a long-standing major goal in polymer chemistry.

2. Computational details

For a complete description of the computational details, including some discussion on the effect of neglecting the counterion, see the Supplementary data.

2.1. Geometry optimization and calculation of thermochemical corrections

All the geometry optimizations were performed using the generalized gradient approximation (GGA) functional BP86 [79–82] as implemented in the Gaussian 03 suite of programs [83]. The SCF solutions were routinely tested for instabilities [84,85], both prior to and subsequent to geometry optimization. All optimized geometries were characterized by the eigenvalues of the analytically obtained second derivatives matrix (Hessian). Thermal corrections to the thermodynamic functions and their kinetic counterparts (in the case of transition states) were computed within standard ideal-gas, rigid-rotor and harmonic oscillator approximations. The temperatures used in the calculation of thermochemical corrections were those reported for the catalytic experiments, 298.15 K (Brookhart complex) and 323.15 K for (Nomura catalyst). The standard state for every reaction species has been chosen as an ideally diluted solution of 1 mol/L concentration (see Supplementary data for the details).

For each stationary point on the potential energy surface, conformational issues were tackled by explicit manual consideration, using DFT, of several of the most reasonable candidate minima.

Effective core potentials (ECPs) of the Stuttgart type were used for all non-hydrogen elements. The ECPs accounted for two inner electrons of C, N and O, and were used in a combination with their corresponding [2s2p] (C, N) and [2s3p] (O) contracted valence basis sets [86]. Similarly, Ru was described by a 28-electron ECP accompanied by a (8s7p6d)/[6s5p3d] contracted valence basis set [87]. Hydrogen atoms were described by a Dunning double-ζ basis set [88].

2.2. Single-point energy evaluations

Single-point (SP) energy evaluations at the optimized geometries were performed using several GGA functionals (BP86 [79–82], PBE [89,90], and BLYP [79,91,92]) as well as a popular and well-tested hybrid-GGA functional (B3LYP [93]) as implemented in the Gaussian 03 suite of programs [83]. The SP energy evaluations using PBE, BLYP and B3LYP were complemented with an empirical dispersion term [94]. A hybrid meta-GGA functional, M06 [95], was also applied, as implemented in NWChem 5.1.1 [96]. In addition

to including dispersion, M06 has been optimized against transition metal chemistry reference data and barrier heights, and shows excellent across-the-board performance in a series of validation studies [97–102]. Unless otherwise indicated, relative energies reported in the following are obtained using the M06 functional.

Whereas the ECPs described above for the geometry optimizations were retained in the SP energy evaluations, the valence basis sets were improved. The valence basis sets for C, N and O were supplemented by single sets of diffuse s and p functions, obtained even-temperedly, and also by polarization d functions (α_d = 0.72 for C; α_d = 0.98 for N; α_d = 1.28 for O). The resulting (5s5p1d) primitive basis sets for C and N were contracted to [4s4p1d], whereas the (5s6p1d) primitive basis set for O was contracted to [4s5p1d]. For Ru, two primitive f functions (α_f = 0.4780, α_f = 1.6660) were added to the (8s7p6d) primitive basis sets. The resulting (8s7p6d2f) primitive basis set was contracted to [7s6p4d2f]. Hydrogen atoms were described by a Dunning triple-ζ basis set [88] augmented by a diffuse, even-tempered s function (α_s = 0.043152) and a polarization p function (α_p = 1.00).

Solvent effects were estimated using the polarizable continuum model (PCM) [103–105] as implemented in Gaussian 03. Toluene was used in the (attempted) polymerizations involving both the Nomura and Brookhart systems, and was thus also chosen for the solvent calculations.

3. Results and discussion

3.1. Direct ethylene insertion for ruthenium propyl cations

The initial hypothesis for the observed difference in activity between **I**/MAO and **III** (Chart 1) is that **III** gives a higher insertion barrier than the analogous complex **II**. In order to test this hypothesis, we have studied the commonly accepted Cossee–Arlman [106,107] mechanism for insertion of ethylene into the ruthenium–propyl bond for monocationic ruthenium ethylene complexes derived from **II** and **III**. The choice of propyl as a model of the growing polymer chain was based on its ability to reproduce agostic interactions which can occur during chain propagation and termination (e.g. [108]). The barrier to insertion was considered to be the Gibbs free energy difference between the insertion transition state structure and the corresponding ethylene propyl complex (Scheme 1). The bare ethylene-free propyl (agostic) complex was assumed to be less stable than the ethylene propyl complex. The latter can thus be considered to be the resting state from which the rate-limiting barrier should be calculated. Evidence for this assumption can be found in the isolation of the ethylene alkyl complex by Dias et al. [28], or in other cationic, late second-row transition metal polymerization catalysts where the ethylene alkyl complexes have been shown to be the resting states of the catalyst [10].

It was shown that the conformational degrees of freedom for the structurally similar Co and Fe bis(imino)pyridine catalysts are several and significant [44,109], and this is indeed also the case for Ru. Four (Nomura) and five (Brookhart) minima for the ruthenium ethylene alkyl complexes were found, and these are denoted as follows: **1a** (ethylene in equatorial position, Fig. 1), **1c** (ethylene in axial position), **1d** (front side β-agostic complex), **1b** (back side β-agostic complex) and **1e** (bipyramidal complex[1]) (cf., Scheme 1). Next, three (Nomura) and two (Brookhart) insertion transition states were located, and denoted: **1c_TS** (backside α-agostic, Fig. 2), **1b_TS** (backside β-agostic) and **1a_TS1** (ethylene in equatorial position) (Scheme 1). The different ethylene alkyl complex conformations cannot, *a priori*, be expected to be in equilibrium since the barriers for such interconversions may be as high as 25 kcal/mol [44,109]. Therefore, we have located the corresponding transition states, denoted **1a–1b_TS**, **1a–1c_TS**, and **1b–1c_TS**. A fourth transition state, linking **1d** with **1c**, denoted **1c–1d_TS** has not been located. This elementary step involves only a minor rearrangement at the metal center and is expected to be associated with a barrier of at most a few kcal/mol above **1c** [109].

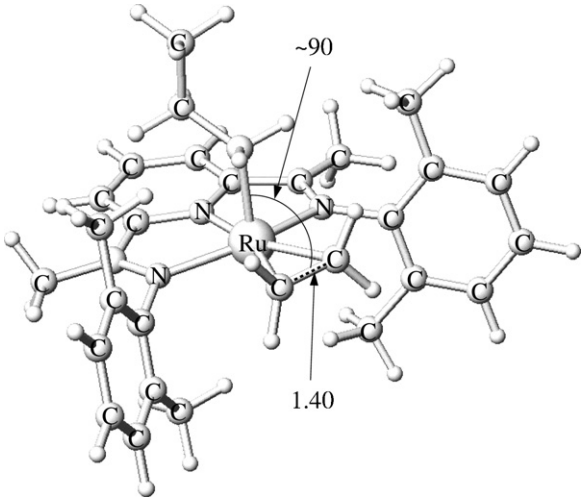

Fig. 1. Geometry for the most stable ethylene complex **1a**, as optimized for the propyl analogue of the Brookhart complex III (Chart 1). Indicated interatomic distance is given in angstroms, angle in degrees.

It is gratifying that the most stable of our calculated structures, the propyl ethylene complex **1a**, corresponds to the methyl ethylene species isolated by Dias et al. [28] (**III**, Chart 1), and this fact lends credibility to our computational approach. In **1a**, the ethylene C–C bond is parallel to the plane of the tridentate ligand (Fig. 1). The perpendicular orientation was found not to be a minimum.

The direct insertion transition state from **1a**, i.e., **1a_TS1** (Scheme 1), has been located, but it is accompanied by a very high relative Gibbs free energy (>45 kcal/mol) in both the Nomura and Brookhart complexes. In case of the Nomura catalyst, **1a_TS1** has lower energy on the triplet energy surface than on the singlet surface, by 8.5 kcal/mol. Nevertheless, the effective barrier to insertion, from **1a** (M = 1) to **1a_TS1** (M = 3), remains prohibitively high (approaching 40 kcal/mol). From Fig. 3 and Table 1 it can be seen that the barriers for conversion between different conformers are of Gibbs free energies comparable to the lowest insertion barrier for the Brookhart complex. For the Nomura complex, the conversion barriers are somewhat lower than the lowest insertion barriers. This is consistent with earlier claims that the conformation conversion barriers are heavily dependent on steric interactions [44,109], which should be higher in complexes carrying the bis(imino)pyridine ligand than in those carrying the pybox ligand. It is thus tempting to think that the higher conversion barriers are responsible for the difference in observed activity. But this seems not to be the case. The Brookhart complex could make the insertion from the resting state by following the sequence **1a**/**1a–1b_TS**/**1b**/**1b–1c_TS**/**1c**/**1c_TS** in which the highest barrier

[1] It should be noted that for the Brookhart complex, the minimum **1e** is very shallow and located along the reaction path linking **1b** and **1a**. It has not been possible to locate this minimum for structures derived from the Nomura catalyst **I** (Table 1), and it is therefore not included in Scheme 1. In Table 3, the label **1e** is used to indicate a (distorted) bipyramidal geometry, i.e., a geometry in which the axial positions are occupied by the imine nitrogen atoms of the bis(imino)pyridine or pybox ligand, and the equatorial positions, which constitute the trigonal plane, by the pyridine nitrogen and the remaining ethylene and propyl ligands.

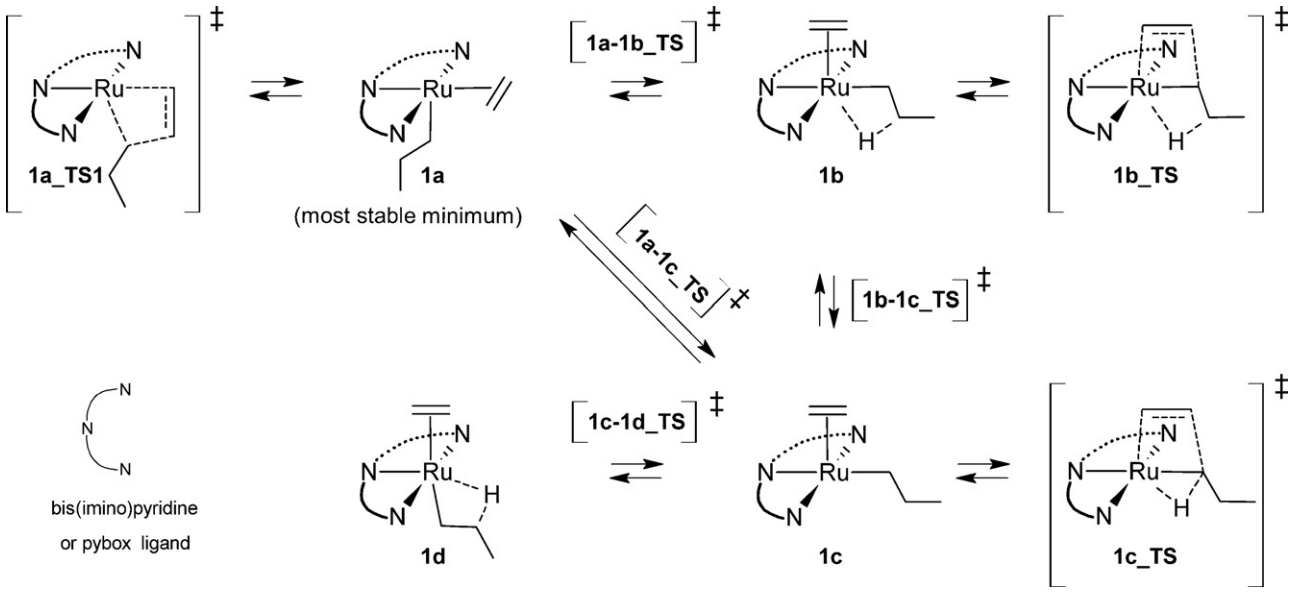

Scheme 1. Mechanism for ethylene insertion as followed when comparing ruthenium propyl cations derived from the Brookhart complex **(III)** and the Nomura catalyst (**I**).

would be the conformational conversion barrier **1b–1c_TS**, with a free energy 26.0 kcal/mol above that of **1a** (Table 2). The analogous Nomura complex, on the other hand, should follow the shorter sequence **1a**/**1a–1b_TS**/**1b**/**1b_TS**, for which the highest barrier is that of insertion, **1b_TS**, with a relative free energy of 25.2 kcal/mol (Fig. 3). Thus, the propagation of **II** is actually found to be slightly more favorable than that of the Brookhart complex **III**, in agreement with observation. However, the minuscule difference in calculated effective propagation barriers should not be taken to be responsible for the difference between activity (Nomura, albeit low) and absence of activity (Brookhart). Moreover, with the current model system, of which neglect of counterion probably is the most important drawback, and computational model (DFT), it does not make sense to address differences in free energy of this magnitude, at least not, as here, those taken between different complexes. We thus have arrived at a first argument for rejecting our number one hypothesis.

In addition, a second argument arises from the fact that the barrier to β-H-transfer to monomer (BHT) is a mere 7.5 kcal/mol (Nomura), cf. the transition state **1d–2d_TS** (Scheme 2). This is much lower than the corresponding insertion barrier (25.2 kcal/mol, transition state **1b_TS**). As is seen for the Nomura complex as well as for other transition metal olefin polymerization catalysts with limited steric hindrance [110–112], a very shallow minimum (**2d**) exists along the double-valley shaped reaction path resembling a bisolefin hydride complex.

Associative termination reactions such as BHT are currently understood to be the most frequent termination reactions for late transition metal coordination–insertion olefin polymerization cat-

Table 1
Relative Gibbs free energies for cationic complexes derived from the Nomura catalyst **I**[a].

$q(M)$[b]	M06	BP86-D	BP86	B3LYP-D	BLYP-D	PBE-D
+1(1)						
1a	0.0	0.0	0.0	0.0	0.0	0.0
1b	5.3	7.7	7.4	7.1	10.1	7.2
1c	13.7	16.5	13.8	15.2	16.8	15.5
1d	3.9	5.7	5.0	4.7	7.7	5.3
1e[c]	–	–	–	–	–	–
1a_TS1	47.6	54.2	49.3	53.8	54.2	52.5
1b_TS	25.2	28.5	26.3	29.6	32.2	27.2
1c_TS	28.0	30.7	24.9	30.3	31.0	28.9
1a–1b_TS	21.6	24.8	22.6	24.5	24.3	24.1
1a–1c_TS	23.6	26.2	24.5	26.1	25.6	25.7
1b–1c_TS	27.1	27.9	25.3	27.2	27.7	27.1
1d–2d_TS	9.3	7.5	9.0	7.6	9.9	7.6
2c	26.9	26.0	23.5	26.4	24.2	26.1
2d	9.3	7.1	8.7	7.1	9.4	7.6
3	22.3	25.5	20.1	24.5	24.6	24.3
3_TS	31.8	35.5	31.0	34.4	34.6	34.5
4a	−1.8	−8.5	8.1	−4.2	−4.5	−6.3
4c	8.0	4.6	20.1	7.1	8.6	6.4
4a_TS1	27.6	25.2	36.5	30.8	30.8	25.2
4a_TS2	28.3	24.1	36.2	30.3	31.4	24.2
4c_TS	30.3	26.8	37.5	30.5	31.0	27.1

[a] See Schemes 1–5 for the species and transformations involved. Reported values are Gibbs free energies in kcal/mol, relative to the monoethylene complex **1a** (Scheme 1).
[b] Charge, q, and spin multiplicity, $M = 2S + 1$, of the complex.
[c] Geometry optimizations lead to **1a**.

Table 2
Relative Gibbs free energies for species related to the Brookhart complex **III**[a].

$q(M)$[b]	M06	BP86-D	BP86	B3LYP-D	BLYP-D	PBE-D
+1 (1)						
1a	0.0	0.0	0.0	0.0	0.0	0.0
1b	13.5	11.9	14.1	12.7	14.7	12.4
1c	18.3	18.9	16.6	19.9	20.0	18.4
1d	7.2	4.4	6.5	7.6	8.0	4.8
1e[c]	24.0	21.9	22.5	24.1	23.5	22.3
1a_TS1	49.9	53.2	48.4	55.0	53.8	52.4
1b_TS[d]	–	–	–	–	–	–
1c_TS	24.9	26.3	22.7	27.8	28.4	25.4
1a–1b_TS	24.2	23.4	23.4	25.3	24.2	23.7
1a–1c_TS	27.8	27.2	25.1	29.8	27.5	27.0
1b–1c_TS	26.0	25.6	24.7	27.6	26.0	25.5
1d–2d_TS	19.8	13.4	16.9	17.0	17.8	14.3
2d[e]	–	–	–	–	–	–
4a	3.5	−5.0	15.3	−1.2	−0.2	−2.3
4c	22.4	15.2	33.2	18.4	20.2	17.5

[a] See Schemes 1–5 for the species and transformations involved. Reported values are Gibbs free energies in kcal/mol, calculated relative to the monoethylene complex 1a (Scheme 1).
[b] Charge, q, and spin multiplicity, $M = 2S + 1$, of the complex.
[c] See footnote 1.
[d] Geometry optimizations lead to a spontaneous rearrangement to yield **1c_TS** (Scheme 1).
[e] Minimum could not be located. Geometry optimizations invariably lead to a ruthenium olefin alkyl complex.

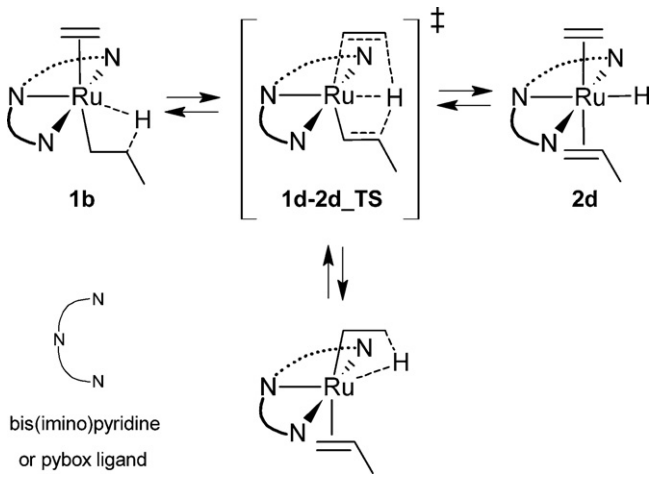

Scheme 2. Mechanism for chain termination via β-hydrogen transfer to the monomer (BHT) when comparing ruthenium propyl cations derived from the Brookhart complex (**III**) and the Nomura catalyst (**I**).

alysts [3,112]. In this reaction, a β-hydrogen is transferred for the growing alkyl chain to an incoming monomer. The alkyl chain now has a terminal olefinic function, which can undergo rotation or decoordination. While rotation can lead to branching, decoordination leads to a termination of the growing polymer chain (Scheme 2). A low barrier to BHT is thus difficult to reconcile with a linear, high M_w polymer as produced by the Nomura catalyst system. In passing, it can be noted that the barrier to BHT for the Brookhart complex is significantly higher, 19.8 kcal/mol, although still well below the effective barrier to chain growth (26.0 kcal/mol) (cf., Fig. 2, Table 2 and Fig. 4).

The above two arguments together strongly suggest that the activity observed for the Nomura catalyst system does not originate from a monocationic alkyl complex operating after the Cossee–Arlman mechanism [106,107].

3.2. Varying the propagation mechanism

Of course, polymeric carbon–carbon bond formation is not limited to the Cossee–Arlman mechanism [106,107]. Migration of an α-H from the Nomura monocationic ruthenium propyl species to form a carbene hydride complex prior to insertion has been proposed as the Green–Rooney mechanism (Scheme 3) [113], but the low stability of this hydride (**2c**) relative to **1a** (26.9 kcal/mol higher in free energy), is already exceeding the barrier for the

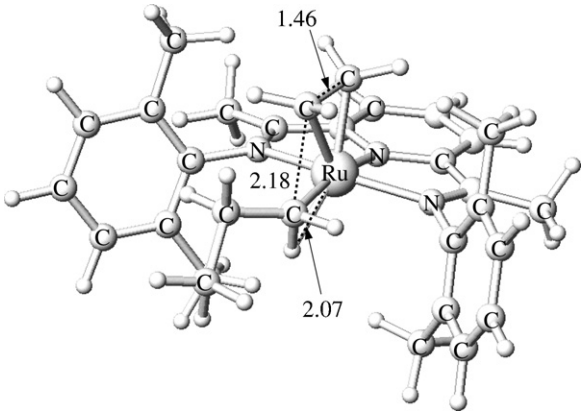

Fig. 2. Transition state for the most facile insertion **1c_TS** as optimized for the propyl analogue of the Brookhart complex III (Chart 1). Indicated interatomic distances are in angstroms.

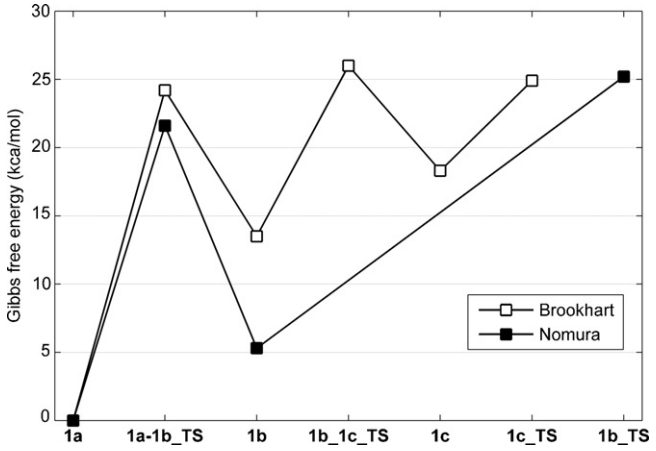

Fig. 3. Gibbs free energy reaction profiles calculated for the propyl cations derived from the Nomura catalyst and the Brookhart complex (Chart 1). The reaction pathways, starting from the most stable ethylene complexes **1a** and leading to the lowest barriers to insertion, are illustrated. See Scheme 1 for structure labels.

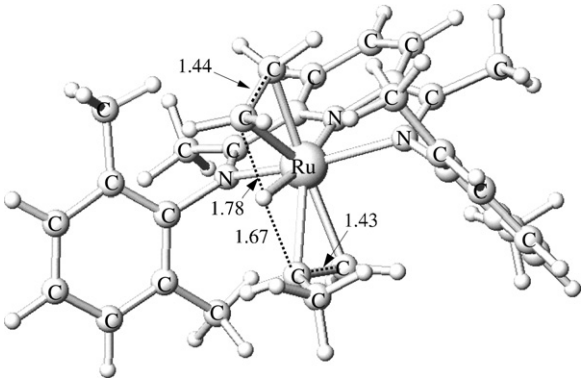

Fig. 4. Transition state for the β-hydrogen transfer to the monomer (BHT) reaction as optimized for the propyl analogue of the Brookhart complex **III** (Chart 1). Indicated interatomic distances are given in angstroms.

most facile Cossee–Arlman insertion (25.2 kcal/mol), making the Green–Rooney pathway seem unlikely (Table 1).

Given the ability of ruthenium to form carbene complexes [29] in combination with known carbene insertion reactions for other late transition metals [114–116], we have also investigated the possibility of inserting an ethyl group into the ruthenium–propylidene bond, via the transition state **3_TS** (Scheme 4). The carbene complex can be thought to arise from an α-H-transfer from the propyl to the incoming ethylene monomer. However, the subsequent barrier to insertion was found to be prohibitively high (31.8 kcal/mol).

A pathway involving direct insertion of ethylene into a carbene, as e.g., proposed by Espelid and Børve in the context of chromium-catalyzed polymerization [117], has also been investigated, but the 1,3-H-transfer necessary to regenerate the carbene from the cyclobutane (not shown) could not be located, the structures in

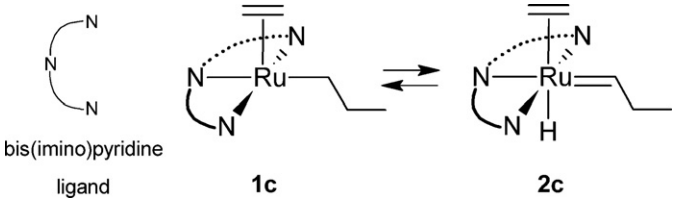

Scheme 3. Metal-hydride formation for a ruthenium propyl complex following the Green–Rooney mechanism.

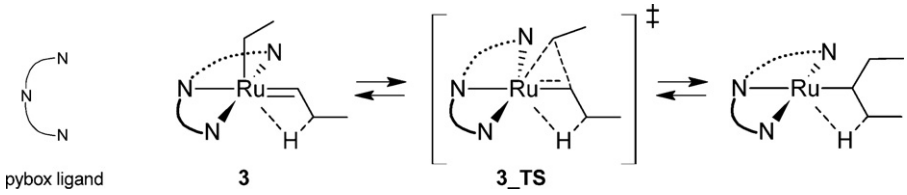

Scheme 4. Alternative carbene propagation mechanism.

this region of the potential energy surface being of very high energies relative to the cyclobutane, most likely due to steric demands of the tridentate ligand.

Insertion involving the coordination of two ethylene monomers may also be envisaged (Scheme 5). It appears that placement of the propyl in axial position (**4a**) is preferred, and this bis(ethylene) complex is more stable (by 1.8 kcal/mol) than the most stable monoethylene complex (**1a**). Two different insertion pathways were followed, one with the propyl in axial position (**4a_TS1**) and one with propyl in equatorial position (**4c_TS**), but both were found to be associated with high (>27 kcal/mol) barriers relative to **1a** (Table 1). An oxidative coupling of two ethylene monomers (**4a_TS2**) was also investigated, starting from **4a**. It was found to be somewhat less favorable than direct insertion, with an effective barrier of 28.3 kcal/mol relative to **1a**.

3.3. Modifying the active species in the Nomura catalyst: changing the formal oxidation state

Given the ability of the bis(imino)pyridine ligand to stabilize a range of oxidation states [54–56], we have re-examined all the above-presented propagation reactions with overall charges on the complexes ranging from +2 to −1, resulting in different formal ruthenium oxidation states. Both low (singlet, doublet) and high (triplet, quartet) spin states were explored. In general, the potential energy surfaces of the high spin states are located at significantly higher energies than their low-spin counterparts. A notable exception is **1a_TS1** for the monocationic species (*vide supra*).

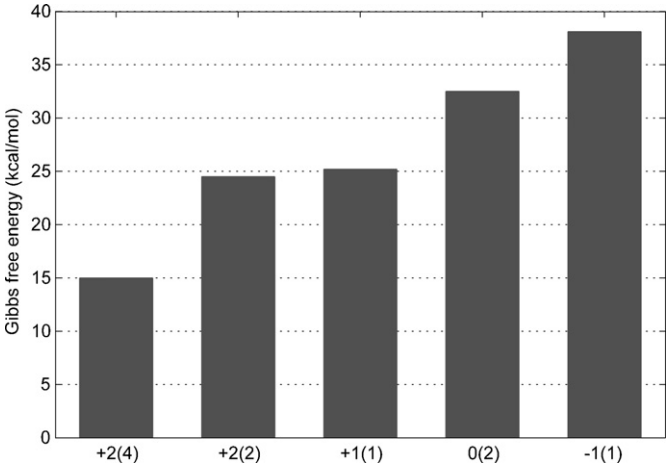

Fig. 5. Gibbs free energy barriers obtained for Cossee–Arlman insertion into the ruthenium–propyl bonds of the complexes derived from the Nomura catalyst (**I**). The barriers have been calculated as the difference between the most stable monoethylene complexes and the lowest-lying transition state for insertion of a single ethylene molecule. The figures underneath the abscissa indicate the charge on the complex and the spin multiplicity (in parenthesis), respectively.

None of the low-spin configurations were found to provide facile insertion via the Cossee–Arlman mechanism, the most promising cases still exhibiting barriers >24 kcal/mol (Table 3). In Fig. 5 it can be seen that the barrier towards insertion is increasing with

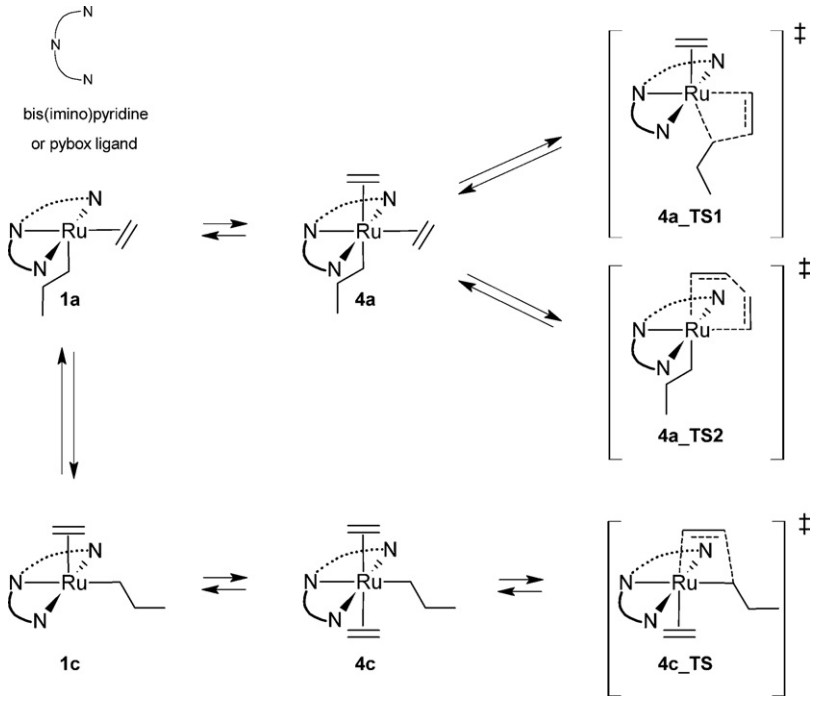

Scheme 5. Various routes to chain propagation involving the coordination of a second ethylene molecule.

Table 3
Relative Gibbs free energies for dicationic, neutral and anionic complexes derived from the Nomura catalyst I[a].

$q(M)$[b]	M06	BP86-D	BP86	B3LYP-D	BLYP-D	PBE-D
+2(2)						
1a	0.0	0.0	0.0	0.0	0.0	0.0
1b	5.4	8.6	8.5	9.3	10.8	7.9
1c	15.0	17.2	15.8	17.5	17.6	16.5
1d	5.0	5.5	5.1	6.9	7.6	5.0
1e[c]	0.3	0.6	0.6	0.9	0.8	0.6
1a_TS1	26.2	26.9	23.4	29.3	28.7	25.5
1b_TS	24.5	26.1	24.2	29.2	29.8	24.7
1c_TS	26.7	27.3	23.9	29.8	29.2	26.0
1d–2d_TS	12.5	9.1	10.4	11.5	11.6	9.4
2c	30.7	29.4	26.8	31.2	27.8	29.4
2d[d]	–	–	–	–	–	–
3	19.8	21.4	15.7	23.2	20.3	19.7
3_TS	25.2	30.3	26.1	29.2	29.7	29.2
4a	4.6	0.2	14.3	2.9	2.1	1.9
4c	10.7	4.8	21.7	9.8	8.4	7.1
4a_TS1	29.0	25.0	36.9	31.4	30.5	25.4
4a_TS2[e]	–	–	–	–	–	–
4c_TS	25.5	22.1	33.5	27.0	27.3	22.4
+2(4)						
1a	0.0	0.0	0.0	0.0	0.0	0.0
1b	−3.2	3.4	1.4	0.1	2.4	2.7
1c	−2.2	4.1	3.3	0.6	3.0	3.9
1d[f]	–	–	–	–	–	–
1e[c]	−3.7	−2.6	−2.9	−2.4	−2.4	−2.8
1a_TS1[g]	–	–	–	–	–	–
1a_TS2	23.4	26.2	23.1	25.2	26.0	25.2
1b_TS	14.5	19.8	18.2	19.6	22.1	18.7
1c_TS	11.4	16.7	13.3	15.8	18.5	15.3
2c[h]	–	–	–	–	–	–
2d[d]	–	–	–	–	–	–
3	12.1	11.5	7.7	14.7	10.8	10.4
3_TS	24.6	25.4	22.7	27.7	25.6	24.7
4a[h]	–	–	–	–	–	–
4c[h]	–	–	–	–	–	–
4a_TS1[h]	–	–	–	–	–	–
4a_TS2[h]	–	–	–	–	–	–
4c_TS[h]	–	–	–	–	–	–
0(2)						
1a	0.0	0.0	0.0	0.0	0.0	0.0
1b	5.8	8.8	6.1	8.7	9.5	7.5
1c	−1.6	−0.9	−1.7	−0.7	−0.9	−1.1
1d	10.0	11.7	10.6	11.4	13.5	11.0
1e[c]	−0.2	0.4	0.1	0.7	0.3	0.3
1a_TS1	40.4	45.1	39.1	45.3	45.3	43.3
1b_TS	34.6	38.5	34.5	39.0	39.7	37.0
1c_TS	31.0	34.1	28.2	35.0	35.1	32.1
1d–2d_TS	15.2	12.7	13.9	14.0	15.2	12.9
2c	34.6	32.5	29.4	33.7	30.4	32.4
2d	15.6	12.1	14.0	13.5	14.2	12.7
3	17.9	19.5	13.4	18.1	17.3	18.3
3_TS	30.9	35.1	30.0	34.0	33.8	34.1
4a	2.7	−2.9	13.6	0.7	0.7	−0.8
4c	12.3	8.5	23.7	11.6	12.5	10.0
4a_TS1[h]	–	–	–	–	–	–
4a_TS2	35.3	30.7	41.6	38.1	37.3	30.2
4c_TS	37.6	33.9	43.9	38.4	38.2	33.8
−1(1)						
1a	0.0	0.0	0.0	0.0	0.0	0.0
1b[f]	–	–	–	–	–	–
1c[f]	–	–	–	–	–	–
1d[i]	–	38.4	37.7	41.8	38.7	37.2
1e[c,f]	–	–	–	–	–	–
1b_TS[j]	–	–	–	–	–	–
1c_TS[j]	–	–	–	–	–	–
1a_TS1	38.1	42.0	38.0	42.2	41.8	40.9
1a_TS2	50.7	44.9	43.8	51.0	46.3	44.2
2c[h]	–	–	–	–	–	–

Table 3 (*Continued*)

$q(M)$[b]	M06	BP86-D	BP86	B3LYP-D	BLYP-D	PBE-D
2d[d]	–	–	–	–	–	–
3	20.5	20.2	16.1	18.8	17.7	19.9
3_TS	34.7	37.7	34.5	37.0	35.9	37.7
4a	17.2	11.0	30.5	14.9	14.1	13.9
4c	26.0	21.0	38.9	25.0	24.7	23.3
4a_TS1[k]	–	–	–	–	–	–
4a_TS2[k]	–	–	–	–	–	–
4c_TS[k]	–	–	–	–	–	–

[a] See Schemes 1–5 for the species and transformations involved. Reported values are relative Gibbs free energies in kcal/mol, relative to the monoethylene complex **1a** (Scheme 1).
[b] Charge, q, and spin multiplicity, $M = 2S + 1$, of the complex.
[c] See footnote 1.
[d] Minimum could not be located. Geometry optimizations invariably lead to a ruthenium olefin alkyl complex.
[e] This transition state, formally leading to a Ru^{V} species, could not be located. However, the energies calculated in the transition region were prohibitively high.
[f] Geometry optimizations lead to a spontaneous rearrangement to yield **1a** (Scheme 1).
[g] Geometry optimizations lead to a spontaneous rearrangement to yield **1c_TS**.
[h] Spontaneous dissociation of ethylene was observed in the geometry optimizations.
[i] M06 value could not be obtained due to SCF convergence problems.
[j] Geometry optimizations lead to spontaneous rearrangement to **1a_TS1**.
[k] Transition states were not located due to the high energy of the olefin complexes.

decreasing positive charge on the complex, which is commensurate with the observation that enchanced π back-donation to ethylene increases the insertion barrier [3,4,118].

Interestingly, for the dicationic complex, ethylene insertion is calculated to be fairly facile on the spin quartet potential energy surface (effective barrier of 14.6 kcal/mol), but the high-spin complexes are consistently found to be located more than 20 kcal/mol higher than their doublet counterparts. In addition, a conventional transition state for BHT, **1d–2d_TS**, could not be located for this spin state, probably due to the lack of empty d-orbitals to accommodate the transferring hydrogen atom. An alternative BHT reaction [112], running via **1a_TS2** (Scheme 6), where no metal-hydride interaction is present, was located instead, but the energy of this transition state was found to be more than 10 kcal/mol higher than the preferred insertion transition state **1a_TS1**. However, due to the modest geometry differences between the quartet and doublet state, the spin quartet state is expected to undergo facile electronic relaxation to reach the lower-lying spin doublet state. Hence, the quartet state is not considered to be responsible for the observed activity. However, it is interesting to note that the high-spin dicationic species appears to be active towards oligomerization and polymerization, which is reminiscent of properties observed for the Fe bis(imino)pyridine catalysts [39,40,50].

Chain propagation involving carbene complexes (Scheme 4) is found to be energetically costly (free energy barrier >25 kcal/mol for **3_TS**). It becomes competitive, however, with the Cossee–Arlman mechanism for dicationic (spin doublet), neutral and anionic complexes (Table 3).

3.4. Modifying the active species in the Nomura catalyst: formation of metallacycles

Another possibility for polymeric carbon–carbon bond formation is a mechanism involving metallacyclic intermediates, as has been demonstrated for homogeneous Cr [119–124], Ti [125–131] and Ta [132–134] trimerization catalysts, as well as homogeneous Cr tetramerization [135,136] and oligomerization [122,137,138] catalysts. The selectivity for trimerization over oligo- or polymerization partly arises from a facile exchange of 1-hexene with ethylene. 1-Hexene is formed after 2,6-H-transfer, which is preferred over subsequent ethylene insertion into metallacyclo-

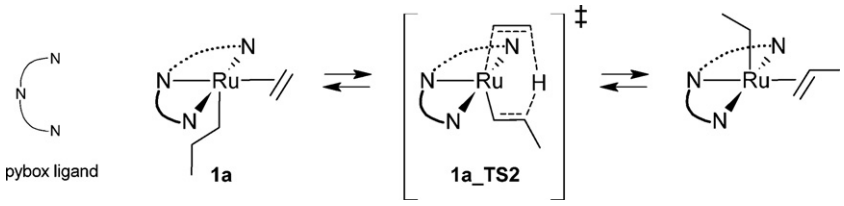

Scheme 6. Alternative mechanism for chain termination via β-hydrogen transfer to the monomer (BHT). **1a_TS2** differs from **1d-2d_TS** in the absence of a metal–hydride interaction.

heptane. It should be noted that, not only oligomerization, but also polymerization through continuously expanding metallacycles could potentially be a realistic possibility for the formation of linear high molecular weight polymer. Polymerization following such a metallacycle mechanism has been suggested for heterogeneous Cr/silica polymerization catalysts [139,140], homogeneous Cr polymerization catalysts [122] and predicted for Hf-based species where 2,6-H-transfer (and, more generally, 2,(6+2n)-H-transfer for larger metallacycles) is disfavored compared to ethylene insertion into the expanding metallacycle, partly due to the strong Hf–C bond [125]. In case of Ru, it is not immediately clear how the different nature of the metal center and the tridentate pybox ligand would influence these preferences. Even if the observed activity would not be due to dealkylated species, it could still be worthwhile exploring the potential of Ru towards selective trimerization since it is a catalytic reaction of considerable commercial interest [141,142].

Dealkylated species (such as **5** and **6**, Scheme 7) can be envisioned to arise from decomposition of a bis(alkyl) species resulting from the dehalogenation and double alkylation by MAO. This decomposition could then involve β-hydrogen transfer and reductive elimination to yield an olefin complex and release methane [125–128,131–133]. Considering the largely unknown effect of MAO, and the minor concentration of the active species, this scenario cannot immediately be dismissed as an unrealistic idea. How minor this concentration might be, can roughly be estimated by assuming that every polymer chain with average weight $M_{w,pol}$ is produced by a single ruthenium center. In this case the polymer mass observed (m) is small compared to the maximum theoretical yield ($m_{\max}$) obtained if all ruthenium centers were to be active:

$$m_{\max} = M_{w,pol} n_{Ru}, \tag{1}$$

where n_{Ru} is the amount of Ru, in moles. Thus, only a tiny fraction, r, of the Ru centers are active:

$$r = \frac{m}{m_{\max}} \approx 10^{-7}. \tag{2}$$

The dealkylated species would then consist of the tridentate ligand with several ethylene monomers, and hence the cationic complex now contains one unpaired electron as opposed to the closed-shell configuration of **II**.

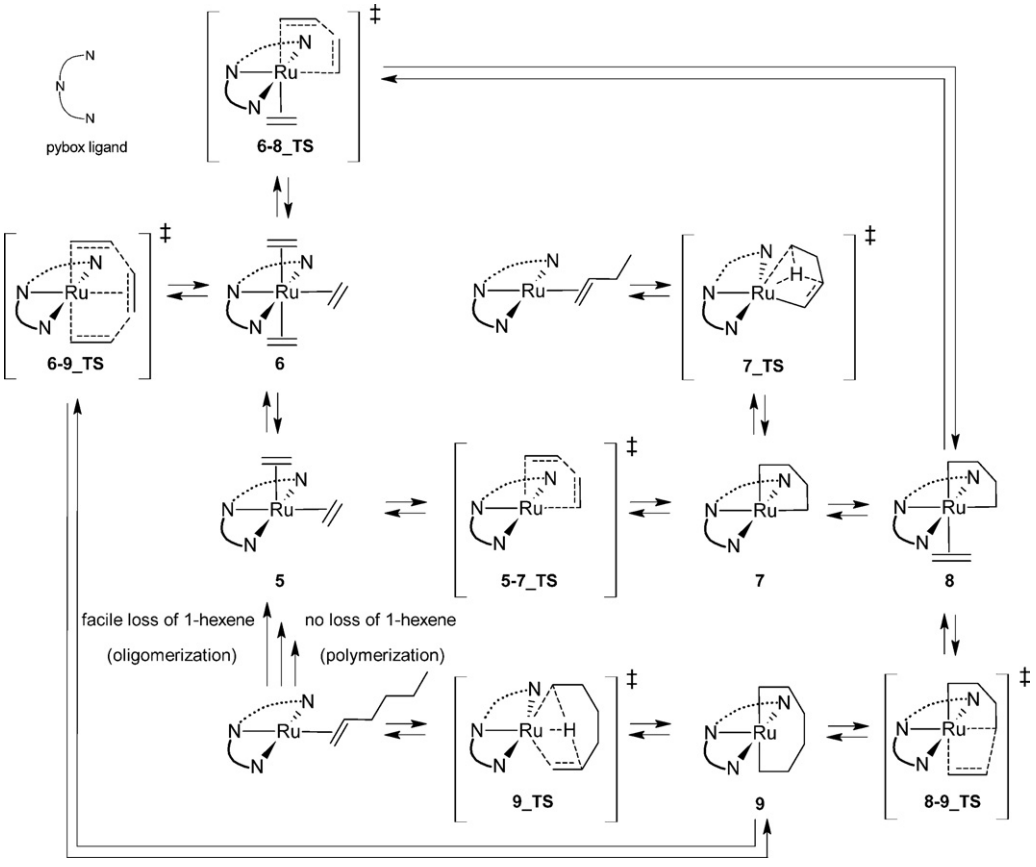

Scheme 7. Various routes to chain propagation involving the formation of metallacycles as investigated in the current work.

Table 4
Relative Gibbs free energies for intermediates and transition states along the metallacycle route (Scheme 7) for complexes derived from the Nomura catalyst **I**[a].

$q(M)$[b]	M06	BP86-D	BP86	B3LYP-D	BLYP-D	PBE-D
0(1)						
5	0.0	0.0	0.0	0.0	0.0	0.0
5–7_TS	17.2	17.9	15.1	18.1	20.2	17.0
7	16.3	17.3	14.3	17.1	19.7	16.3
8	1.5	−4.1	7.6	0.0	0.8	−5.0
8–9_TS	29.4	25.0	33.7	30.4	30.7	23.4
9	1.1	−0.9	5.9	1.9	3.7	−2.9
9_TS	10.1	7.1	13.1	13.5	16.4	4.2
6[c]	–	–	–	–	–	–
7_TS	32.4	32.9	29.9	34.9	36.0	32.0
Overall barrier[d]	*29.4*	*29.2*	*33.7*	*30.4*	*30.7*	*28.5*
−1(2)						
5	0.0	0.0	0.0	0.0	0.0	0.0
5–7_TS	23.2	26.0	22.4	23.7	26.6	24.9
7	9.8	8.7	4.7	7.2	8.1	8.1
8	−1.1	−7.5	4.7	−4.0	−2.9	−8.1
8–9_TS	33.4	31.8	39.6	34.1	36.1	30.2
9	0.3	−2.0	4.6	10.6	8.4	11.7
9_TS	15.5	14.6	20.2	18.5	22.7	11.8
6[c]	–	–	–	–	–	–
7_TS	35.3	35.6	32.0	36.9	38.4	34.6
Overall barrier[d]	*34.5*	*39.3*	*39.6*	*38.0*	*38.9*	*38.3*
+1(2)						
5	0.0	0.0	0.0	0.0	0.0	0.0
5–7_TS	14.9	17.5	13.3	18.0	19.3	16.2
7	12.3	15.8	11.2	15.7	18.3	14.2
8	5.5	4.3	14.3	8.1	8.9	2.9
8–9_TS	28.2	24.3	32.5	31.6	31.0	22.5
9	1.5	3.0	7.8	5.2	8.5	0.2
9_TS	3.2	2.0	7.9	8.2	11.8	−1.1
6	7.8	−1.1	17.1	3.3	2.7	−0.1
7_TS	31.2	33.5	28.0	35.3	36.4	32.0
Overall barrier[d]	*28.2*	*24.3*	*32.5*	*31.6*	*31.0*	*22.5*
+2(1)						
5	0.0	0.0	0.0	0.0	0.0	0.0
5– 7_TS	18.9	21.2	17.4	22.8	22.5	20.2
7	15.5	18.4	13.4	20.1	20.6	16.8
8	15.6	10.4	21.4	20.7	18.5	9.1
8–9_TS	34.4	28.7	36.9	38.6	35.1	27.3
9	1.6	2.4	6.9	7.2	8.4	−0.5
9_TS	1.8	−0.1	5.9	6.5	9.3	−3.1
6	−9.8	−17.2	−0.3	−12.7	−13.9	−16.1
6–9_TS	20.6	16.1	28.3	23.9	23.8	15.1
6–8_TS	19.4	14.5	26.9	23.6	21.6	13.6
7_TS	29.2	29.0	25.3	34.1	33.3	27.6
Overall barrier[d]	*30.4*	*33.3*	*28.6*	*36.6*	*37.8*	*31.3*

[a] Reported values are Gibbs free energies in kcal/mol, relative to the bisolefinic complex **5** (Scheme 7).
[b] Charge, q, and spin multiplicity, $M = 2S + 1$, of the complex.
[c] During geometry optimization, a spontaneous dissociation of ethylene was observed, yielding **5** (Scheme 7).
[d] Overall Gibbs free energy barrier for completing a trimerization cycle.

Fig. 6 shows the Gibbs free energy profiles for the complexes with different charge, beginning with the diethylene complex **5**, followed by the oxidative coupling, **5–7_TS**, the ethylene metallacyclopentane complex **7**, the insertion of ethylene into metallacyclopentane **8–9_TS**, and, finally, the metallacycloheptane **9**. Concerted 2,4-H-transfer barriers have been calculated for all metallacyclopentane **7** complexes, but, possibly due to the induced strain, these were found to be prohibitively high (>30 kcal/mol).

It appears that all considered pathways can be excluded as candidate explanations for the observed activity (Fig. 6 and Table 4). The anionic complex shows too high barrier to oxidative coupling, transition state **5–7_TS**, as well as to insertion, **8–9_TS**. The neutral and cationic complexes display barriers to oxidative coupling **5–7_TS** below 20 kcal/mol, but the neutral complex shows an effective insertion barrier of more than 25 kcal/mol. It appears that the cationic complex has the lowest overall barrier through this reaction path, thanks to a relatively low insertion barrier compared to that of the neutral complex. The insertion transition state **9_TS** for the dicationic species is accompanied by a fairly low barrier (ca. 15 kcal/mol), but due to the limited stability of **8**, the overall barrier becomes >30 kcal/mol. So the cationic complex has the lowest overall barrier, 28.2 kcal/mol, of all the compounds for which a metallacycle mechanism was followed.

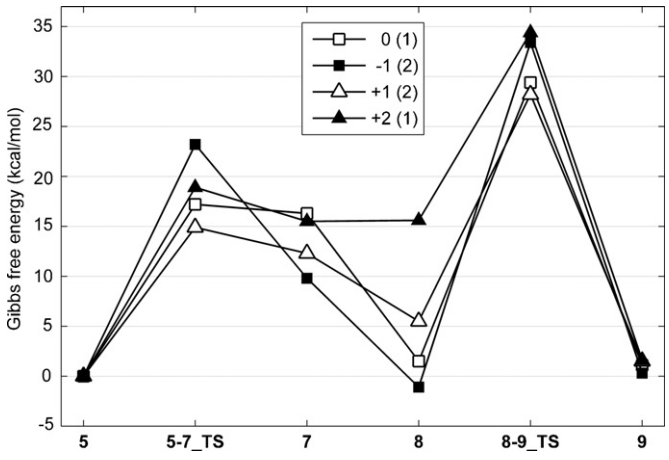

Fig. 6. Gibbs free energy reaction profiles of the metallacyclic reaction pathway (Scheme 7) for complexes derived from the Nomura catalyst (**I**). The figures in the legend indicate the charge on the complex and the spin multiplicity (in parenthesis), respectively.

It should be noted that, for the dicationic complex, **6** is far more stable (9.8 kcal/mol) than **5**. In other words, the dicationic complexes cannot be expected to follow this reaction pathway. Instead, a concerted oxidative coupling of the three ethylene monomers can take place, with all three located at close distance from the Ru metal center (**6–9_TS**). This reaction has a calculated barrier of 30.4 kcal/mol, and could not be located for the cationic, neutral and anionic complexes.

Since all species have modest 2,6-H-transfer barriers, decoordination might lead to selective trimerization. However, the high relative Gibbs free energy of the rate-limiting insertion barrier, due to the transition state **8–9_TS**, is detrimental to the catalytic activity. No or only low activity is predicted for the considered species (Table 4). Trimerization is thus hampered by the same bottleneck as the Cossee–Arlman-style linear chain growth, namely the difficult insertion of ethylene into a ruthenium–alkyl bond.

4. Conclusion

Comparable barrier heights (25.2 and 26.0 kcal/mol, respectively) have been calculated for the Cossee–Arlman-style ethylene insertion into the metal–propyl bond in cationic ruthenium complexes derived from **II** and **III**. For **III**, it is found that the conformational interconversion barriers are slightly (by ca. 1 kcal/mol) higher than the insertion barrier, and thus appear to be rate-limiting. For **II**, on the other hand, the interconversion barriers are calculated to be located well below the insertion barriers, suggesting that steric interactions are mainly responsible for the interconversion barriers. This result underlines the importance of this type of reactions when studying polymerization catalysts decorated by realistic, potentially bulky ligands. Whereas the methyl ethylene complex **III** bearing a bis(imino)pyridine ligand is inactive toward ethylene polymerization, the analogous pybox complex **II**

would be the result of a standard activation of **I** by MAO. Our calculations thus strongly suggest that the catalytic activity observed for **I**/MAO does not originate from chain growth following the standard Cossee–Arlman mechanism for a ruthenium alkyl monocation analogous to those established for olefin polymerization catalysts of Group 4 or 10 transition metals. We thus embarked on an extensive search for candidate active species generated by **I**/MAO, following the reaction profiles of basically all the known mechanisms for metal-mediated olefin polymerization. In addition, several different oxidation and spin states of the active species were considered for each mechanism. In the bulk of the cases, the barriers to chain growth were found to be high and at best comparable (24.5 kcal/mol for Cossee–Arlman insertion by dicationic propyl species) to those calculated in the initial part of the study directed toward ruthenium propyl monocations. In the case of quartet dicationic species however, a reasonable barrier to chain growth via Cossee–Arlman insertion (18.2 kcal/mol) was obtained. This is reminiscent of previous findings for the Fe bis(imino)pyridine catalysts [39,40,50]. However, the promotion needed to generate the corresponding active quartet complexes was found to be costly, leading to prohibitively large effective barriers, i.e., adding the cost of promotion to the insertion barrier. The overall conclusion from our calculations thus is that the activity toward ethylene polymerization observed for **I**/MAO most probably does not originate from a mononuclear ruthenium complex bearing an intact pybox ligand. Instead, a range of different modifications of the ligand, either chemical modifications such as alkylation, (de)protonation or dimerization, or bidentate coordination modes, could, possibly, explain the observed activity, as could complexes involving more than one metal center. Finally, the potential of Ru pybox species towards selective trimerization should be very low, as activities are hampered by the same bottleneck as the linear chain-growth via the Cossee–Arlman mechanism, namely a slow insertion of ethylene into a ruthenium–alkyl bond.

Supplementary data available

Detailed computational details, total energies, thermochemical corrections, dispersion corrections, solvent corrections, Cartesian coordinates of the reported optimized geometries, and details on the treatment of standard states.

Acknowledgements

The Norwegian Research Council (NFR) is acknowledged for financial support through the GASSMAKS (Grant No. 182536) and KOSK (Grant No. 177322) programmes as well as for CPU resources granted through the NOTUR supercomputing programme. The University of Bergen is acknowledged for financial support through the Nanoscience programme.

Appendix A. Supplementary data

Supplementary data associated with this article can be found, in the online version, at doi:10.1016/j.molcata.2010.03.023.

References

[1] K. Ziegler, E. Holzkamp, H. Breil, H. Martin, Angew. Chem. Int. Ed. 67 (1955) 541–547.
[2] G. Natta, Angew. Chem. Int. Ed. 68 (1956) 393–403.
[3] R. Schmid, T. Ziegler, Organometallics 19 (2000) 2756–2765.
[4] V.R. Jensen, W. Thiel, Organometallics 20 (2001) 4852–4862.
[5] S.D. Ittel, L.K. Johnson, M. Brookhart, Chem. Rev. 100 (2000) 1169–1203.
[6] G.J.P. Britovsek, V.C. Gibson, D.F. Wass, Angew. Chem. Int. Ed. 38 (1999) 429–447.
[7] V.C. Gibson, S.K. Spitzmesser, Chem. Rev. 103 (2003) 283–315.
[8] L.S. Boffa, B.M. Novak, Chem. Rev. 100 (2000) 1479–1493.
[9] A. Sen, S. Borkar, J. Organomet. Chem. 692 (2007) 3291–3299.
[10] L.K. Johnson, C.M. Killian, M. Brookhart, J. Am. Chem. Soc. 117 (1995) 6414–6415.
[11] L.K. Johnson, S. Mecking, M. Brookhart, J. Am. Chem. Soc. 118 (1996) 267–268.
[12] C.M. Killian, D.J. Tempel, L.K. Johnson, M. Brookhart, J. Am. Chem. Soc. 118 (1996) 11664–11665.
[13] S. Mecking, L.K. Johnson, L. Wang, M. Brookhart, J. Am. Chem. Soc. 120 (1998) 888–899.
[14] E. Drent, R. van Dijk, R. van Ginkel, B. van Oort, R.I. Pugh, Chem. Commun. (2002) 744–745.
[15] E. Drent, R. van Dijk, R. van Ginkel, B. van Oort, R.I. Pugh, Chem. Commun. (2002) 964–965.
[16] W. Weng, Z. Shen, R.F. Jordan, J. Am. Chem. Soc. 129 (2007) 15450–15451.
[17] S. Luo, J. Vela, G.R. Lief, R.F. Jordan, J. Am. Chem. Soc. 129 (2007) 8946–8947.
[18] T. Kochi, K. Yoshimura, K. Nozaki, Dalton Trans. (2006) 25–27.
[19] T. Kochi, S. Noda, K. Yoshimura, K. Nozaki, J. Am. Chem. Soc. 129 (2007) 8948–8949.
[20] K.M. Skupov, P.R. Marella, M. Simard, G.P.A. Yap, N. Allen, D. Conner, B.L. Goodall, J.P. Claverie, Macromol. Rapid Commun. 28 (2007) 2033–2038.
[21] T.R. Younkin, E.F. Connor, J.I. Henderson, S.K. Friedrich, R.H. Grubbs, D.A. Bansleben, Science 287 (2000) 460–462.
[22] A.W. Waltman, T.R. Younkin, R.H. Grubbs, Organometallics 23 (2004) 5121–5123.
[23] G.J.P. Britovsek, V.C. Gibson, B.S. Kimberley, P.J. Maddox, S.J. McTavish, G.A. Solan, A.J.P. White, D.J. Williams, Chem. Commun. (1998) 849–850.
[24] G.J.P. Britovsek, M. Bruce, V.C. Gibson, B.S. Kimberley, P.J. Maddox, S. Mastroianni, S.J. McTavish, C. Redshaw, G.A. Solan, S. Strömberg, A.J.P. White, D.J. Williams, J. Am. Chem. Soc. 121 (1999) 8728–8740.
[25] G.J.P. Britovsek, V.C. Gibson, S.K. Spitzmesser, K.P. Tellmann, A.J.P. White, D.J. Williams, J. Chem. Soc., Dalton Trans. (2002) 1159–1171.
[26] M.J. Fullana, M.J. Miri, S.S. Vadhavkar, N. Kolhatkar, A.C. Delis, J. Polym. Sci., Part A: Polym. Chem. 46 (2008) 5542–5558.
[27] B.L. Small, M. Brookhart, A.M.A. Bennett, J. Am. Chem. Soc. 120 (1998) 4049–4050.
[28] E.L. Dias, M. Brookhart, P.S. White, Organometallics 19 (2000) 4995–5004.
[29] T.M. Trnka, R.H. Grubbs, Acc. Chem. Res. 34 (2001) 18–29.
[30] S.J. McTavish, M.J. Payne, PCT Int. Appl., WO 2001023396 (2001).
[31] V.C. Gibson, B.S. Kimberley, P.J. Maddox, S. Mastroianni, PCT Int. Appl., WO 99-GB2888 19990901 (2000).
[32] W. Hirahata, M. Itagaki, K. Nomura, Eur. Pat. Appl., EP 942010 (1999).
[33] G. BASF A.-G., Ger. Offen. (2004), WO 2004041796 (2004).
[34] M.W. Holtcamp, T.T. Wenzel, G.T. Whiteker, PCT Int. Appl., WO 2001083569 (2001).
[35] K. Nomura, S. Warit, Y. Imanishi, Macromolecules 32 (1999) 4732–4734.
[36] Y. Imanishi, K. Nomura, J. Polym. Sci. Part A: Polym. Chem. (2000) 4613–4626.
[37] K. Nomura, S. Warit, Y. Imanishi, Bull. Chem. Soc. Jpn. 73 (2000) 599–605.
[38] E.Y.X. Chen, T.J. Marks, Chem. Rev. 100 (2000) 1391–1434.
[39] R. Raucoules, T. de Bruin, P. Raybaud, C. Adamo, Organometallics 28 (2009) 5358–5367.
[40] R. Raucoules, T. de Bruin, P. Raybaud, C. Adamo, Organometallics 27 (2008) 3368–3377.
[41] P.M. Castro, P. Lahtinen, K. Axenov, J. Viidanoja, T. Kotiaho, M. Leskela, T. Repo, Organometallics 24 (2005) 3664–3670.
[42] M.W. Bouwkamp, E. Lobkovsky, P.J. Chirik, J. Am. Chem. Soc. 127 (2005) 9660–9661.
[43] D.V. Khoroshun, D.G. Musaev, T. Vreven, K. Morokuma, Organometallics 20 (2001) 2007–2026.
[44] L.Q. Deng, P. Margl, T. Ziegler, J. Am. Chem. Soc. 121 (1999) 6479–6487.
[45] E.A.H. Griffiths, G.J.P. Britovsek, V.C. Gibson, I.R. Gould, Chem. Commun. (1999) 1333–1334.
[46] M.W. Bouwkamp, S.C. Bart, E.J. Hawrelak, R.J. Trovitch, E. Lobkovsky, P.J. Chirik, Chem. Commun. (2005) 3406–3408.
[47] K.P. Bryliakov, E.P. Talsi, N.V. Semikolenova, V.A. Zakharov, Organometallics 28 (2009) 3225–3232.
[48] J. Scott, S. Gambarotta, I. Korobkov, P.H.M. Budzelaar, Organometallics 24 (2005) 6298–6300.
[49] Y.V. Kissin, C.T. Qian, G.Y. Xie, Y.F. Chen, J. Polym. Sci. Part A: Polym. Chem. 44 (2006) 6159–6170.
[50] V.L. Cruz, J. Ramos, J. Martínez-Salazar, S. Gutiérrez-Oliva, A. Toro-Labbé, Organometallics 28 (2009) 5889–5895.
[51] A.A. Barabanov, G.D. Bukatov, V.A. Zakharov, N.V. Semikolenova, T.B. Mikenas, L.G. Echevskaja, M.A. Matsko, Macromol. Chem. Phys. 207 (2006) 1368–1375.
[52] A.A. Barabanov, G.D. Bukatov, V.A. Zakharov, N.V. Semikolenova, L.G. Echevskaja, M.A. Matsko, Macromol. Chem. Phys. 206 (2005) 2292–2298.
[53] J. Martínez, V. Cruz, J. Ramos, S. Gutiérrez-Oliva, J. Martínez-Salazar, A. Toro-Labbé, J. Phys. Chem. C 112 (2008) 5023–5028.
[54] P.H.M. Budzelaar, B. de Bruin, A.W. Gal, K. Wieghardt, J.H. van Lenthe, Inorg. Chem. 40 (2001) 4649–4655.
[55] B. de Bruin, E. Bill, E. Bothe, T. Weyhermuller, K. Wieghardt, Inorg. Chem. 39 (2000) 2936–2947.
[56] D. Enright, S. Gambarotta, G.P.A. Yap, P.H.M. Budzelaar, Angew. Chem. Int. Ed. 41 (2002) 3873–3876.
[57] E.P. Talsi, D.E. Babushkin, N.V. Semikolenova, V.N. Zudin, V.N. Panchenko, V.A. Zakharov, Macromol. Chem. Phys. 202 (2001) 2046–2051.

[58] E.P. Talsi, K.P. Bryliakov, N.V. Semikolenova, V.A. Zakharov, M. Bochmann, Kinet. Catal. 48 (2007) 490–504.
[59] K.P. Bryliakov, N.V. Semikolenova, V.A. Zakharov, E.P. Talsi, Organometallics 23 (2004) 5375–5378.
[60] K.P. Bryliakov, N.V. Semikolenova, V.N. Zudin, V.A. Zakharov, E.P. Talsi, Catal. Commun. 5 (2004) 45–48.
[61] J. Scott, S. Gambarotta, I. Korobkov, P.H.M. Budzelaar, J. Am. Chem. Soc. 127 (2005) 13019–13029.
[62] D. Reardon, F. Conan, S. Gambarotta, G. Yap, Q.Y. Wang, J. Am. Chem. Soc. 121 (1999) 9318–9325.
[63] H. Sugiyama, G. Aharonian, S. Gambarotta, G.P.A. Yap, P.H.M. Budzelaar, J. Am. Chem. Soc. 124 (2002) 12268–12274.
[64] G.K.B. Clentsmith, V.C. Gibson, P.B. Hitchcock, B.S. Kimberley, C.W. Rees, Chem. Commun. (2002) 1498–1499.
[65] I.J. Blackmore, V.C. Gibson, P.B. Hitchcock, C.W. Rees, D.J. Williams, A.J.P. White, J. Am. Chem. Soc. 127 (2005) 6012–6020.
[66] I. Khorobkov, S. Gambarotta, G.P.A. Yap, P.H.M. Budzelaar, Organometallics 21 (2002) 3088–3090.
[67] M. Bruce, V.C. Gibson, C. Redshaw, G.A. Solan, A.J.P. White, D.J. Williams, Chem. Commun. (1998) 2523–2524.
[68] T.M. Kooistra, D.G.H. Hetterscheid, E. Schwartz, Q. Knijnenburg, P.H.M. Budzelaar, A.W. Gal, Inorg. Chim. Acta 357 (2004) 2945–2952.
[69] H. Sugiyama, S. Gambarotta, G.P.A. Yap, D.R. Wilson, S.K.H. Thiele, Organometallics 23 (2004) 5054–5061.
[70] H. Sugiyama, I. Korobkov, S. Gambarotta, A. Moller, P.H.M. Budzelaar, Inorg. Chem. 43 (2004) 5771–5779.
[71] K.G. Orrell, A.G. Osborne, V. Sik, M.W. daSilva, J. Organomet. Chem. 530 (1997) 235–246.
[72] M.L. Creber, K.G. Orrell, A.G. Osborne, V. Sik, A.L. Bingham, M.B. Hursthouse, J. Organomet. Chem. 631 (2001) 125–134.
[73] J.A. Olson, R. Boyd, J.W. Quail, S.R. Foley, Organometallics 27 (2008) 5333–5338.
[74] J. Scott, S. Gambarotta, I. Korobkov, Q. Knijnenburg, B. de Bruin, P.H.M. Budzelaar, J. Am. Chem. Soc. 127 (2005) 17204–17206.
[75] M.P. Coles, R.F. Jordan, J. Am. Chem. Soc. 119 (1997) 8125–8126.
[76] G. Talarico, V. Busico, P.H.M. Budzelaar, Organometallics 20 (2001) 4721–4726.
[77] G. Talarico, P.H.M. Budzelaar, Organometallics 21 (2002) 34–38.
[78] R.J. Meier, E. Koglin, J. Phys. Chem. A 105 (2001) 3867–3874.
[79] A.D. Becke, Phys. Rev. A 38 (1988) 3098–3100.
[80] J.P. Perdew, A. Zunger, Phys. Rev. B 23 (1981) 5048–5079.
[81] J.P. Perdew, W. Yue, Phys. Rev. B 33 (1986) 8800–8802.
[82] J.P. Perdew, Phys. Rev. B 34 (1986) 7406–17406.
[83] M.J. Frisch, G.W. Trucks, H.B. Schlegel, G.E. Scuseria, M.A. Robb, J.R. Cheeseman, J.J.A. Montgomery, T. Vreven, K.N. Kudin, J.C. Burant, J.M. Millam, S.S. Iyengar, J. Tomasi, V. Barone, B. Mennucci, M. Cossi, G. Scalmani, N. Rega, G.A. Petersson, H. Nakatsuji, M. Hada, M. Ehara, K. Toyota, R. Fukuda, J. Hasegawa, M. Ishida, T. Nakajima, Y. Honda, O. Kitao, H. Nakai, M. Klene, X. Li, J.E. Knox, H.P. Hratchian, J.B. Cross, C. Adamo, J. Jaramillo, R. Gomperts, R.E. Stratmann, O. Yazyev, A.J. Austin, R. Cammi, C. Pomelli, J.W. Ochterski, P.Y. Ayala, K. Morokuma, G.A. Voth, P. Salvador, J.J. Dannenberg, V.G. Zakrzewski, S. Dapprich, A.D. Daniels, M.C. Strain, O. Farkas, D.K. Malick, A.D. Rabuck, K. Raghavachari, J.B. Foresman, J.V. Ortiz, Q. Cui, A.G. Baboul, S. Clifford, J. Cioslowski, B.B. Stefanov, G. Liu, A. Liashenko, P. Piskorz, I. Komaromi, R.L. Martin, D.J. Fox, T. Keith, M.A. Al-Laham, C.Y. Peng, A. Nanayakkara, M. Challacombe, P.M.W. Gill, B. Johnson, W. Chen, M.W. Wong, C. Gonzalez, J.A. Pople, Gaussian 03, Gaussian, Inc., Pittsburg PA, 2003.
[84] R. Seeger, J.A. Pople, J. Chem. Phys. 66 (1977) 3045–3050.
[85] R. Bauernschmitt, R. Ahlrichs, J. Chem. Phys. 104 (1996) 9047–9052.
[86] A. Bergner, M. Dolg, W. Kuchle, H. Stoll, H. Preuss, Mol. Phys. 80 (1993) 1431–1441.
[87] D. Andrae, U. Haussermann, M. Dolg, H. Stoll, H. Preuss, Theor. Chim. Acta 77 (1990) 123–141.
[88] T.H. Dunning Jr., P.J. Hay, in: H.F. Schaefer III (Ed.), Methods of Electronic Structure Theory, Plenum Press, New York, 1977, pp. 1–27.
[89] J.P. Perdew, K. Burke, M. Ernzerhof, Phys. Rev. Lett. 77 (1996) 3865–3868.
[90] J.P. Perdew, K. Burke, M. Ernzerhof, Phys. Rev. Lett. 78 (1997) 1396–11396.
[91] C. Lee, W. Yang, R.G. Parr, Phys. Rev. B 37 (1988) 785–789.
[92] B. Miehlich, A. Savin, H. Stoll, H. Preuss, Chem. Phys. Lett. 157 (1989) 200–206.
[93] A.D. Becke, J. Chem. Phys. 98 (1993) 5648–5652.
[94] S. Grimme, J. Comput. Chem. 27 (2006) 1787–1799.
[95] Y. Zhao, D.G. Truhlar, Theor. Chem. Acc. 120 (2008) 215–241.
[96] E.J. Bylaska, W.A.d. Jong, N. Govind, K. Kowalski, T.P. Straatsma, M. Valiev, D. Wang, E. Apra, T.L. Windus, J. Hammond, P. Nichols, S. Hirata, M.T. Hackler, Y. Zhao, P.-D. Fan, R.J. Harrison, M. Dupuis, D.M.A. Smith, J. Nieplocha, V. Tipparaju, M. Krishnan, Q. Wu, T.V. Voorhis, A.A. Auer, M. Nooijen, E. Brown, G. Cisneros, G.I. Fann, H. Fruchtl, J. Garza, K. Hirao, R. Kendall, J.A. Nichols, K. Tsemekhman, K. Wolinski, J. Anchell, D. Bernholdt, P. Borowski, T. Clark, D. Clerc, H. Dachsel, M. Deegan, K. Dyall, D. Elwood, E. Glendening, M. Gutowski, A. Hess, J. Jaffe, B. Johnson, J. Ju, R. Kobayashi, R. Kutteh, Z. Lin, R. Littlefield, X. Long, B. Meng, T. Nakajima, S. Niu, L. Pollack, M. Rosing, G. Sandrone, M. Stave, H. Taylor, G. Thomas, J.v. Lenthe, A. Wong, Z. Zhang, NWChem, A Computational Chemistry Package for Parallel Computers, Pacific Northwest National Laboratory, Richland, Washington, 2007.
[97] N. Sieffert, M. Bühl, Inorg. Chem 48 (2009) 4622–4624.
[98] Y. Zhao, D.G. Truhlar, Acc. Chem. Res. 41 (2008) 157–167.
[99] Y. Minenkov, G. Occhipinti, V.R. Jensen, J. Phys. Chem. A 113 (2009) 11833–11844.
[100] T. van Mourik, J. Chem. Theor. Comput. 4 (2008) 1610–1619.
[101] C.J. Cramer, D.G. Truhlar, Phys. Chem. Chem. Phys. 11 (2009) 10757–10816.
[102] Y. Zhao, D.G. Truhlar, J. Chem. Theor. Comput. 5 (2009) 324–333.
[103] J. Tomasi, Theor. Chem. Acc. 112 (2004) 184–203.
[104] J. Tomasi, B. Mennucci, R. Cammi, Chem. Rev. 105 (2005) 2999–3093.
[105] M. Cossi, G. Scalmani, N. Rega, V. Barone, J. Chem. Phys. 117 (2002) 43–54.
[106] P. Cossee, J. Catal. 3 (1964) 80–88.
[107] E.J. Arlman, P. Cossee, J. Catal. 3 (1964) 99–104.
[108] V.R. Jensen, D. Koley, M.N. Jagadeesh, W. Thiel, Macromolecules 38 (2005) 10266–10278.
[109] P. Margl, L.Q. Deng, T. Ziegler, Organometallics 18 (1999) 5701–5708.
[110] L.H. Shultz, D.J. Tempel, M. Brookhart, J. Am. Chem. Soc. 123 (2001) 11539–11555.
[111] M.D. Leatherman, S.A. Svejda, L.K. Johnson, M. Brookhart, J. Am. Chem. Soc. 125 (2003) 3068–3081.
[112] G. Talarico, P.H.M. Budzelaar, Organometallics 27 (2008) 4098–4107.
[113] K.J. Ivin, J.J. Rooney, C.D. Stewart, M.L.H. Green, R. Mahtab, J. Chem. Soc. Chem. Commun. (1978) 604–606.
[114] E. Jellema, P.H.M. Budzelaar, J.N.H. Reek, B. de Bruin, J. Am. Chem. Soc. 129 (2007) 11631–11641.
[115] D.G.H. Hetterscheid, C. Hendriksen, W.I. Dzik, J.M.M. Smits, E.R.H. van Eck, A.E. Rowan, V. Busico, M. Vacatello, V.V. Castelli, A. Segre, E. Jellema, T.G. Bloemberg, B. de Bruin, J. Am. Chem. Soc. 128 (2006) 9746–9752.
[116] E. Jellema, A.L. Jongerius, J.N.H. Reek, B. De Bruin, Chem. Soc. Rev. (2010), doi:10.1039/b911333a.
[117] Ø. Espelid, K.J. Børve, J. Catal. 195 (2000) 125–139.
[118] P. Margl, L.Q. Deng, T. Ziegler, J. Am. Chem. Soc. 120 (1998) 5517–5525.
[119] J.R. Briggs, J. Chem. Soc. Chem. Commun. (1984) 674–675.
[120] R. Emrich, O. Heinemann, P.W. Jolly, C. Krüger, G.P.J. Verhovnik, Organometallics 16 (1997) 1511–1513.
[121] T. Agapie, S.J. Schofer, J.A. Labinger, J.E. Bercaw, J. Am. Chem. Soc. 126 (2004) 1304–1305.
[122] A.K. Tomov, J.J. Chirinos, D.J. Jones, R.J. Long, V.C. Gibson, J. Am. Chem. Soc. 127 (2005) 10166–10167.
[123] W.J. van Rensburg, C. Grové, J.P. Steynberg, K.B. Stark, J.J. Huyser, P.J. Steynberg, Organometallics 23 (2004) 1207–1222.
[124] T. Agapie, J.A. Labinger, J.E. Bercaw, J. Am. Chem. Soc. 129 (2007) 14281–14295.
[125] S. Tobisch, T. Ziegler, J. Am. Chem. Soc. 126 (2004) 9059–9071.
[126] P.J.W. Deckers, B. Hessen, J.H. Teuben, Angew. Chem. Int. Ed. 40 (2001) 2516–2517.
[127] P.J.W. Deckers, B. Hessen, J.H. Teuben, Organometallics 21 (2002) 5122–5135.
[128] C. Pellecchia, D. Pappalardo, L. Oliva, M. Mazzeo, G.J. Gruter, Macromolecules 33 (2000) 2807–2814.
[129] A.N.J. Blok, P.H.M. Budzelaar, A.W. Gal, Organometallics 22 (2003) 2564–2570.
[130] T.J.M. de Bruin, L. Magna, P. Raybaud, H. Toulhoat, Organometallics 22 (2003) 3404–3413.
[131] S. Tobisch, T. Ziegler, Organometallics 22 (2003) 5392–5405.
[132] C. Andes, S.B. Harkins, S. Murtuza, K. Oyler, A. Sen, J. Am. Chem. Soc. 123 (2001) 7423–7424.
[133] Z.X. Yu, K.N. Houk, Angew. Chem. Int. Ed. 42 (2003) 808–811.
[134] R. Arteaga-Müller, H. Tsurugi, T. Saito, M. Yanagawa, S. Oda, K. Mashima, J. Am. Chem. Soc. 131 (2009) 5370–5371.
[135] M.J. Overett, K. Blann, A. Bollmann, J.T. Dixon, D. Haasbroek, E. Killian, H. Maumela, D.S. McGuinness, D.H. Morgan, J. Am. Chem. Soc. 127 (2005) 10723–10730.
[136] S. Kuhlmann, J.T. Dixon, M. Haumann, D.H. Morgan, J. Ofili, O. Spuhl, N. Taccardi, P. Wasserscheid, Adv. Synth. Catal. 348 (2006) 1200–1206.
[137] A.K. Tomov, J.J. Chirinos, R.J. Long, V.C. Gibson, M.R.J. Elsegood, J. Am. Chem. Soc. 128 (2006) 7704–7705.
[138] D.S. McGuinness, J.A. Suttil, M.G. Gardiner, N.W. Davies, Organometallics 27 (2008) 4238–4247.
[139] E. Groppo, C. Lamberti, S. Bordiga, G. Spoto, A. Zecchina, Chem. Rev. 105 (2005) 115–183.
[140] Ø. Espelid, K.J. Børve, J. Catal. 206 (2002) 331–338.
[141] J.T. Dixon, M.J. Green, F.M. Hess, D.H. Morgan, J. Organomet. Chem. 689 (2004) 3641–3668.
[142] D.F. Wass, Dalton Trans. (2007) 816–819.